THE EUROPEAN SOCIETY OF MEDICINE
Medical Research Archives, Volume 14 Issue 1

RESEARCH ARTICLE

Investigation of the landscape of RSV M protein with quercetin and acetylated quercetin in the search for antivirals

Luana Seixas [1], Renan Pereira Pedro [1], Jéssica Maróstica de Sá [1], Jefferson de Souza Busso [1], Mikael Santana dos Santos [1], João Victor Piloto [1], Luis Octavio Regasini [2], Ícaro Putinhon Caruso [1], Marcelo Andres Fossey [1], Fátima Pereira de Souza [1]

[1] Department of Physics,Multiuser Center for Biomolecular Innovation (CMIB), Institute of Biosciences, Humanities and Exact Sciences (IBILCE) São Paulo State University "Júlio de Mesquita Filho" (UNESP), 15054-000 São José do Rio Preto, SP, Brazil
[2] Department of Chemistry and Environmental Sciences, Institute of Biosciences, Humanities and Exact Sciences (IBILCE) São Paulo State University "Júlio de Mesquita Filho" (UNESP), 15054-000 São José do Rio Preto, SP, Brazil

OPEN ACCESS

PUBLISHED
31 January 2026

CITATION
Seixas, L., Pedro, RP., et al., 2026. Investigation of the landscape of RSV M protein with quercetin and acetylated quercetin in the search for antivirals. Medical Research Archives, [online] 14(1).

DOI

ISSN
2375-1924

ABSTRACT

Human Respiratory Syncytial Virus (hRSV) is a major causative agent of severe respiratory infections in infants, the elderly and immuno-compromised individuals. The hRSV genome synthesizes eleven proteins, two of which are non-structural. Among its structural proteins, the matrix (M) protein plays a pivotal role in viral assembly and budding, making it a strategic target for the development of novel antiviral approaches. In this study, we investigated the interaction of the M protein with quercetin, a natural flavonoid, as well as with two acetylated derivatives, peracetylated quercetin and tetraacetylated quercetin, using spectroscopic techniques in combination with computational biophysics methods. The results showed specific interactions in a 1:1 stoichiometry, characterized through moderate affinity and a predominance of hydrophobic forces. Acetylation enhanced conformational stability and increased the binding affinity of the complexes, with peracetylated quercetin exhibiting the strongest capacity for molecular recognition. Molecular dynamics simulations supported these findings, showing that chemical modification introduced additional contact points, including new hydrogen bonds, thereby conferring greater structural stability to the complexes. Overall, these findings contribute to the understanding of the molecular mechanisms that regulate the interaction between the M protein and small ligands and point to acetylated flavonoids as potential antiviral candidates capable of interfering with hRSV assembly and maturation processes.

Keywords: Matrix protein; hRSV; quercetin; acetylated quercetin

1. Introduction

Human Respiratory Syncytial Virus (hRSV) is a major cause of lower respiratory tract infections (LRTIs) in children and elderly [1]. In pediatric populations, hRSV infection frequently manifests as bronchiolitis and is strongly associated with an increased risk of asthma later in life [2]. Among children under five years of age, hRSV remains one of the principal viral pathogens linked to pneumonia [3]. On a global scale, hRSV-associated acute lower respiratory infections (ALRIs) were estimated, in 2019, to account for around 33 million cases, leading to 3.6 million hospital admissions and 130,000 deaths [4].

The hRSV belongs to the family Pneumoviridae and species *Orthopneumovirus hominis* [5]. It is an enveloped virus [6] with helical symmetry [7] and can display spherical, filamentous or pleomorphic forms [8]. Its genome is a non-segmented, single-stranded, negative-sense RNA of approximately 15,200 nucleotides, encoding two non-structural proteins (NS1 and NS2) and nine structural proteins. These include the surface glycoproteins F, G and SH, the nucleocapsid proteins N, P and L, the nucleocapsid-associated proteins M2-1 and M2-2 and the matrix protein M [6].

The M protein consists of 256 amino acids arranged into two domains, N-terminal and C-terminal. The N-terminal domain adopts a horseshoe-like shape, while the C-terminal domain forms a flattened barrel structure. Both are largely composed of β-sheets and are linked with a flexible loop of 13 residues [9]. The native form of M is a dimer, stabilized through the interaction of the N-terminal region of one protomer with the C-terminal region of the other. Hydrophobic regions at the interdomain connection point to a requirement for oligomerization and interactions with other proteins in order to achieve stability [10]. Furthermore, phosphorylation of residue Thr205 modulates M oligomerization and regulates its nucleocytoplasmic trafficking [11]. Functionally, M is a phosphorylated, non-glycosylated protein located just beneath the viral envelope, where it bridges the lipid bilayer to the nucleocapsid [12]. During early stages of infection, M is directed to the host nucleus through Importin β1, where it disrupts host transcription [13,14]. At later stages, it is exported back to the cytoplasm via CRM-1, where it associates with M2-1 and the ribonucleocapsid (RNP) and participates in the formation of viral inclusion bodies (IBs) [15–17]. M interacts with glycoprotein G in the Golgi and subsequently with F at lipid rafts in the plasma membrane, coordinating the transition from viral transcription to assembly and budding [18–21].

Despite advances in vaccine development, treatment options for hRSV remain limited. At the moment, treatment consists of the use of monoclonal antibodies, such as palivizumab and nirsevimab and the broad-spectrum antiviral Ribavirin, which has a high cost, variable efficacy and various adverse effects [22]. Recently, three vaccines have been approved, two protein subunit vaccines, RSVPreF3 (Arexvy®, GSK) and RSVPreF (Abrysvo®, Pfizer) and one mRNA vaccine, mRNA-1345 (mRESVIA, Moderna) [23]. These vaccines are licensed for adults over 60 years of age, with Abrysvo® also approved for maternal immunization to provide passive protection to infants during their first six months of life [24]. However, the lack of broadly effective antivirals highlights the urgent need for new therapeutic strategies [25].

In this context, natural compounds such as flavonoids have attracted attention as potential antiviral agents [26]. Among them, quercetin (Q) is one of the most widely studied and has shown inhibitory effects against viruses including influenza, rhinovirus and human immunodeficiency virus [27–30]. Quercetin has also demonstrated activity against RSV, reducing both infection and replication [31,32]. Acetylated derivatives of quercetin have shown even greater potential, for example, quercetin pentaacetate has been reported to inhibit RSV adhesion *in vitro* more effectively than the unmodified compound [33]. The acetylation is known to enhance cellular uptake, protect molecules from metabolic degradation and improve both bioactivity and bioavailability [34–40].

Based on this premise, we aimed to explore the interaction between the hRSV M protein and quercetin along with two of its acetylated derivatives, peracetylated quercetin (Q1) and tetraacetylated quercetin (Q2). The chemical structures of these compounds are illustrated in Figure 1. Comparing these derivatives, our objective is to understand how acetylation boosts the antiviral properties of quercetin and to aid in the strategic development of new hRSV therapeutic options.

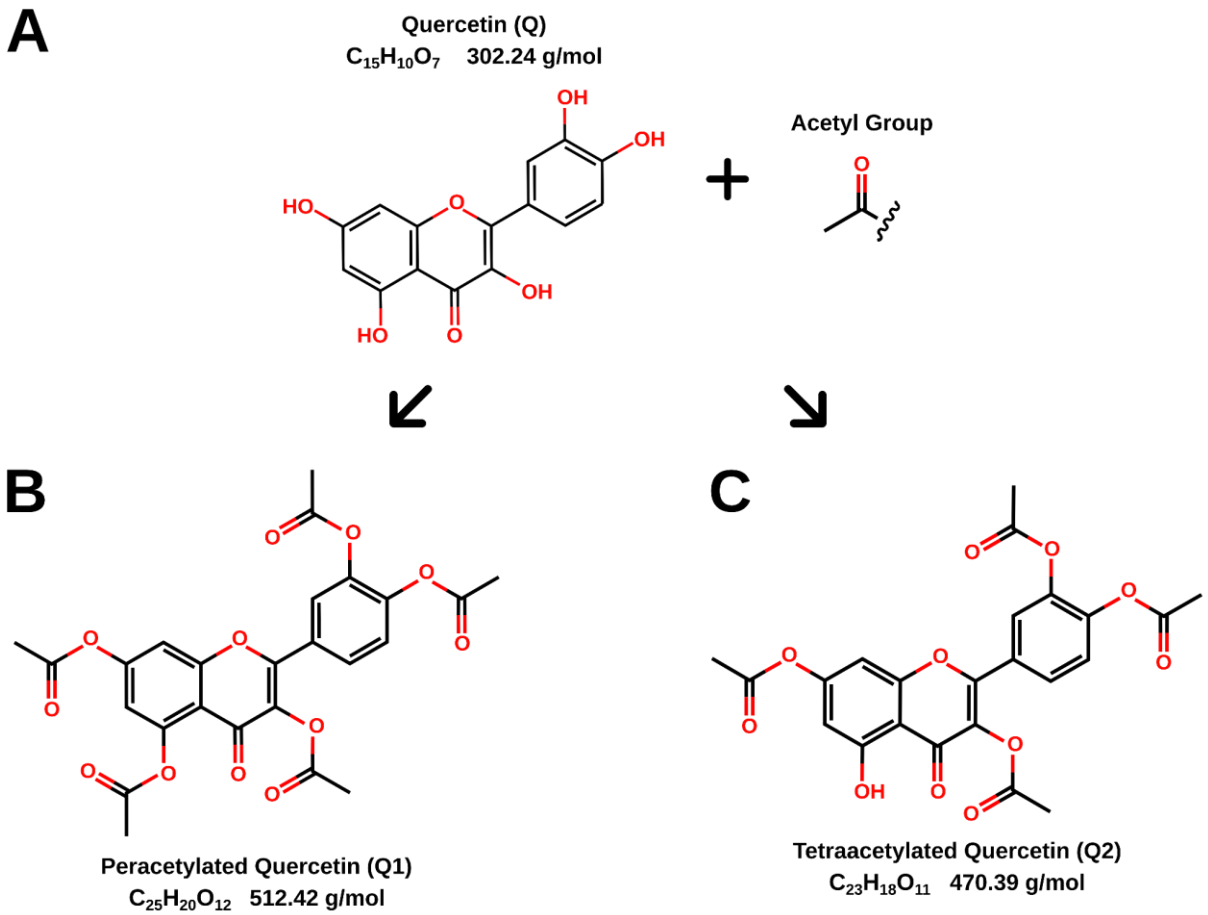

Figure 1: Chemical structures of quercetin and its acetylated derivatives. **(A)** Quercetin **(B)** Peracetylated quercetin (Q1), and **(C)** Tetraacetylated quercetin (Q2).

2. Materials and Methods

a. EXPRESSION AND PURIFICATION OF RECOMBINANT M PROTEIN

The gene encoding the M domain of the M protein, which consists of 256 amino acid residues, was synthesized by DNA 2.0 (ATUM) and then inserted into the pD441-NHT-M expression vector. Plasmid transformation was performed in Escherichia coli BL21, using kanamycin (25 µg/mL) and chloramphenicol (37 µg/mL). Transformed colonies were inoculated into liquid LB broth supplemented with antibiotics and cultivated at 37 °C under agitation (100 rpm) for 4 hours. Recombinant expression was induced adding IPTG (0.4 mM) when the optical density at 600 nm (OD_{600}) reached 0.7. The culture was subsequently incubated at 28 °C with agitation (120 rpm) for 16 hours. Following induction, cells were harvested via centrifugation (4500 rpm, 4 °C, 30 min) and the cell pellet was resuspended in lysis buffer (20 mM Tris-HCl, 500 mM NaCl, 5% glycerol, 0.1% Triton X-100, 1 mM β-mercaptoethanol, pH 7.5), supplemented with lysozyme (1 mg/mL) and phenylmethylsulfonyl fluoride (PMSF, 0.5 mM). Cell lysis was carried out through sonication using six cycles of 30 s pulses (2 s on, 1 s off), interspersed with 40 s intervals in an ice bath. The lysate was subjected to centrifugation (17000 rpm, 4 °C, 40 min) and the resulting supernatant was filtered through 0.45 µm membranes prior to purification. Recombinant protein was initially purified through affinity chromatography using a Ni-NTA column pre-equilibrated with binding buffer (20 mM Tris-HCl, 500 mM NaCl, 5 mM imidazole, 1 mM β-mercaptoethanol, pH 8). Elution was performed using an imidazole gradient (10 mM to 1 M). To facilitate buffer exchange and remove contaminants, the eluate was subjected to size-exclusion chromatography. Protein purity was assessed using sodium dodecyl sulphate-polyacrylamide gel electrophoresis (SDS-PAGE, 15%) under denaturing conditions. Protein concentration was determined spectrophotometrically applying the Beer-Lambert Law, measuring absorbance at 280 nm and using a molar extinction coefficient of 27,390 M^{-1} cm^{-1} [9] .

b. FLAVONOIDS

Quercetin (2-(3,4-dihydroxyphenyl)-3,5,7-trihydroxy-chromen-4-one) was purchased from Sigma-Aldrich (St. Louis, MO, USA). Quercetins acetylations were performed as previous described. Flavonoid stock solutions were prepared in a mix comprising 5% Milli-Q water and 95% ethanol (EtOH). Concentrations were determined in UV-Vis spectroscopy measurements were performed using a Cary-3E spectrophotometer (Varian, Palo Alto, CA) with quartz cuvettes featuring a 1 cm optical path length, according to the Beer-Lambert law [41], using the specific molar extinction coefficients: quercetin (Q), ε_{376} = 21,880 M^{-1} cm^{-1} (λ = 376 nm) [42]; peracetylated quercetin (Q1), ε_{266} = 29,305 M^{-1} cm^{-1} (λ = 266 nm); and tetraacetylated quercetin (Q2), ε_{268} = 21,720 M^{-1} cm^{-1} (λ = 268 nm) [38].

c. FLUORESCENCE SPECTROSCOPY

The interaction between hRSV M protein and the ligands was assessed using fluorescence spectroscopy, monitoring the quenching of intrinsic tryptophan fluorescence upon ligand addition. Experiments were conducted on an ISS PC1 spectrofluorometer (Champaign, IL, USA) equipped with a quartz cuvette (1 cm optical path length) and a

NESLab RTE-221 thermal bath (Thermo Electron Corporation, USA). The excitation and emission slit widths were adjusted to 1.0 mm. Excitation was performed at 295 nm to selectively excite the tryptophan residues of the protein and emission spectra were recorded in the 300-500 nm range with ten accumulations. Fluorescence quenching assays were carried out via titrating the ligands (until 20 µM) into a constant protein concentration (5 µM). Measurements were performed at 288, 298 and 308 K. The protein remained in its native state throughout the studied temperature range, as the melting temperature of hRSV M protein is approximately 317 K [43]. To minimize internal filtering effects and obtain a more reliable estimate of the emitted fluorescence, we applied the following equation (Eq. 1):

$$F_{corr} = F_{obs}\, x\, 10^{(A_{\lambda ex} + A_{\lambda em})/2} \quad (1)$$

In this expression, F_{corr} denotes the corrected fluorescence intensity, whereas F_{obs} represents the experimentally measured value. The terms $A_{\lambda ex}$ and $A_{\lambda em}$ correspond to the absorbance values recorded at the excitation and emission wavelengths, respectively [44].

To distinguish the quenching mechanisms and quantify binding events, the fluorescence data were analyzed with well-established models. First, the Stern-Volmer relationship (Eq. 2) was applied to determine whether quenching followed a dynamic or static profile:

$$\frac{F_0}{F} = 1 + k_q \tau_0 [L] = 1 + K_{SV}[L] \quad (2)$$

where F_0 and F are the fluorescence intensities in the absence and presence of ligand, respectively, τ_0 is the lifetime of the fluorophore in the absence of quencher, $[L]$ is the ligand concentration, k_q is the bimolecular quenching constant and K_{SV} the Stern-Volmer constant.

Binding affinity and stoichiometry were then obtained using fitting the data to a double-logarithmic model (Eq. 3), which provides both the number of ligands bound per protein molecule (n) and the binding constant (K_b):

$$log\left(\frac{F_0 - F}{F}\right) = n(K_b) - nlog\left(\frac{1}{[L_t]} - \frac{F_0 - F}{F_0}[P_t]\right) \quad (3)$$

where $[L_t]$ and $[P_t]$ correspond to the total ligand and protein concentrations, respectively.
Finally, to explore the driving forces of the interaction, thermodynamic parameters were derived using the Van't Hoff equation (Eq. 4):

$$\Delta G = -RT\, ln(K_b) = \Delta H - T\Delta S \quad (4)$$

where R is the gas constant ($1.98\ cal\ mol^{-1}\ K^{-1}$), T is the absolute temperature and K_b the binding constant. The resulting values of ΔG, ΔH and $T\Delta S$ allowed us to infer whether complex formation was mainly driven by enthalpic contributions, such as hydrogen bonding, or by entropic effects, typically associated with hydrophobic interactions.

d. MOLECULAR DOCKING AND MOLECULAR DYNAMICS

The interactions between the molecules and the M protein of the hRSV were assessed through molecular docking using the CB-Dock2 server [45,46], employing the crystallographic model of the M protein (PDB ID: 2VQP [47]) as the initial structure. Blind docking was performed for each compound to identify the most representative binding pose, characterized through the lowest interaction energy. The three-dimensional structures of the ligands and their corresponding topology files were generated using the CHARMM-GUI server [48,49]. The highest-ranked docking model was employed as the initial structure for molecular dynamics simulations, conducted using the GROMACS 2020.3 package [50], with the CHARMM36 force field and the TIP3P water model [51–53]. Energy minimization was performed in two steps, 50,000 steps using the steepest descent algorithm, followed by 5,000 steps using the conjugate gradient method, both without positional restraints. Equilibration was carried out in two 100 ps phases, the first with restraints applied to both protein and ligand and the second without restraints. Production simulations were conducted for 450 ns with a 2 fs integration time step, at 298 K, 1 atm pressure and a physiological saline concentration of 0.15 M. Coordinates and energies were recorded every 100 ps. The Parrinello-Rahman barostat and Berendsen thermostat were employed [54,55]. The simulation box was defined as a 10 Å buffer from the protein surface under periodic boundary conditions. Trajectory analysis was performed using GROMACS-integrated tools. The conformation exhibiting the lowest short-range interaction energy was selected as the representative structure of the M protein/ligand complex.

3. Results and Discussion

a. LIGAND-INDUCED FLUORESCENCE QUENCHING OF THE HRSV M PROTEIN

To elucidate the interaction between the hRSV M protein and quercetin (Q) and its acetylated derivatives (Q1 and Q2), we performed intrinsic fluorescence experiments, exploiting selective tryptophan excitation at 295 nm (see *Materials and Methods* for details). The M protein exhibited a maximal emission around 340 nm, a value typical of tryptophan residues partially exposed to the solvent [56,57]. Upon addition of Q, a concentration-dependent decrease in fluorescence intensity was observed (Figure 2A). A similar pattern was noted for Q1 and Q2 (Figure 2B and C), indicating that all these compounds act as tryptophan fluorescence quenchers and, consequently, interact directly with the M protein.

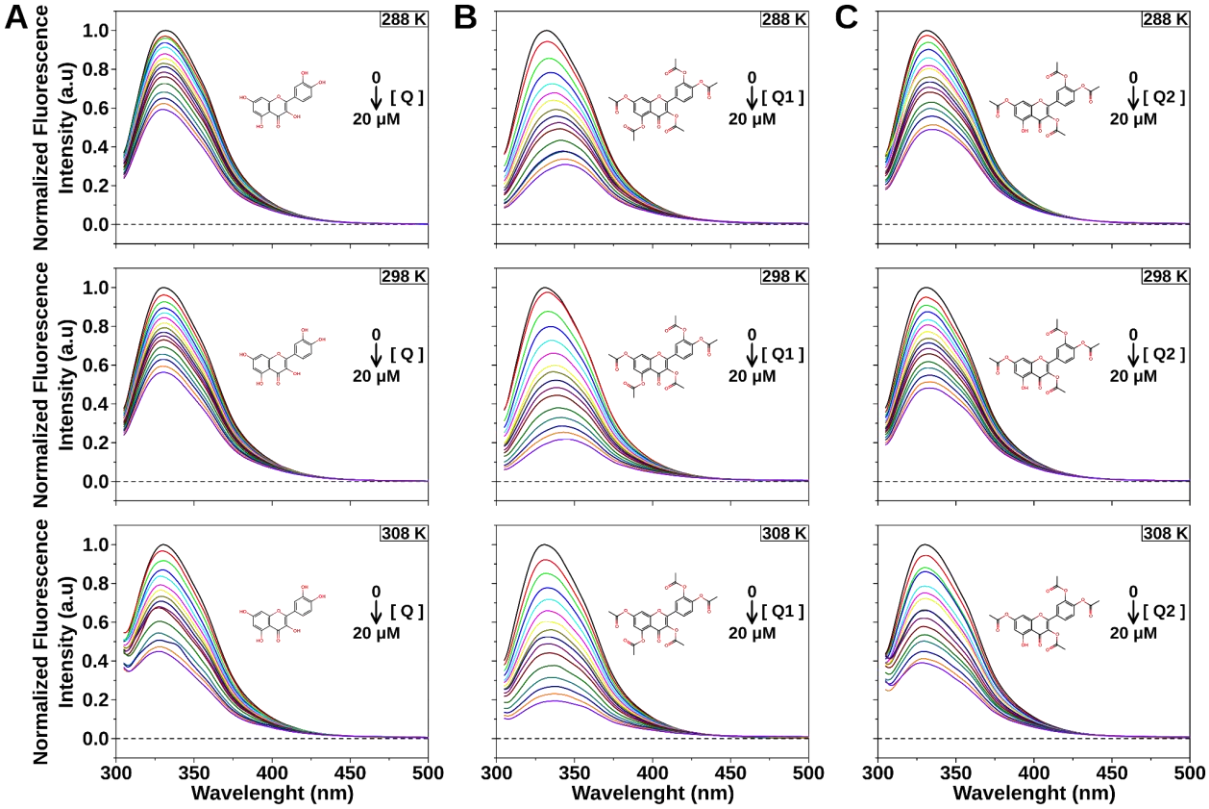

Figure 2: Fluorescence emission spectra of the hRSV M protein in the presence of ligands **(A)** Q, **(B)** Q1, and **(C)** Q2. Measurements were performed with excitation at 295 nm, and each ligand was titrated stepwise from 0 to 20 µM into a 5 µM protein solution at 288 K, 298 K, and 308 K.

Although the emission maximum wavelength did not undergo significant shifts, the quenching efficiency varied among the compounds, reflecting differences in their interaction strengths. To further characterize the nature of this process, the data were analyzed using the Stern-Volmer equation (Eq. 2) across different temperatures (Figure 3).

The curves obtained for quercetin revealed that quenching increased with rising temperature, suggesting a dynamic mechanism in which collisions between the fluorophore and quencher occur more frequently under warmer conditions. In contrast, the acetylated derivatives exhibited a distinct behavior, the quenching curves showed minimal temperature dependence, remaining nearly constant in some instances [42]. These findings point to a static quenching mechanism, associated with the formation of stable complexes with the M protein [57].

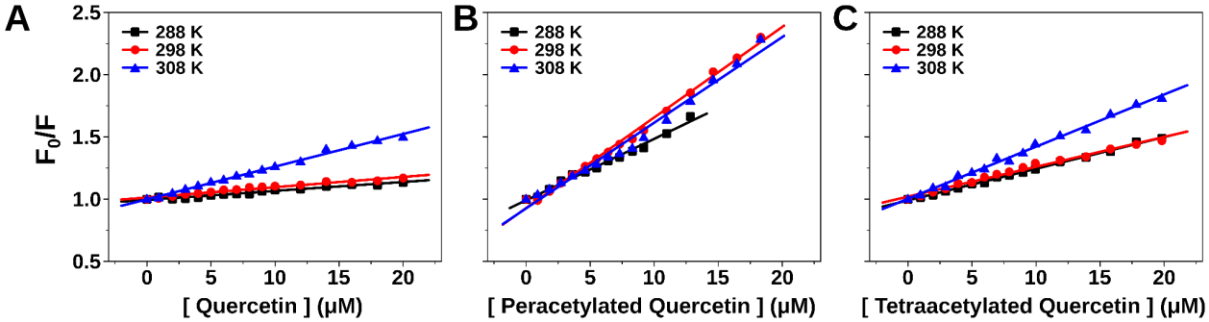

Figure 3: Stern-Volmer plots depicting the quenching of the intrinsic fluorescence of M protein as a function of ligand concentration: **(A)** Q, **(B)** Q1, and **(C)** Q2. The curves were recorded at 288, 298, and 308 K.

b. BINDING CONSTANTS AND LIGAND SPECIFICITY OF THE HRSV M PROTEIN

The interaction of the hRSV M protein with quercetin and its acetylated derivatives was investigated using the double-logarithmic equation (Eq. 3)[58], applied to the fluorescence quenching data obtained experimentally (Figure 2). Fitting the experimental data with this model revealed consistent trends across the different ligands examined. These results are shown in Figure 4.

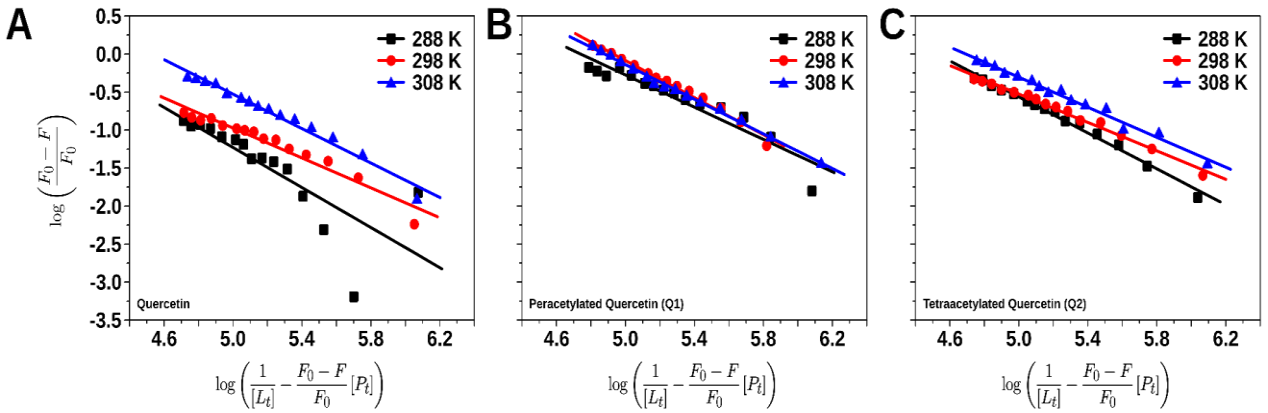

Figure 4: Double-logarithmic plots derived from fluorescence titrations of protein M with **(A)** Q, **(B)** Q1, and **(C)** Q2. Titrations were performed at different temperatures, 288 K (black squares), 298 K (red circles) and 308 K (blue triangles). The solid lines represent the linear fits, enabling the determination of the parameters *n* and K_b, as defined in Eq. 3.

The values of *n* and K_b are summarized in Table 1, enabling a systematic comparison of the distinct experimental conditions.

Table 1: Binding site number (*n*), binding constant (K_b) and Stern-Volmer constant (K_{SV}) determined for quercetin and acetylated derivatives under different thermal conditions.

Ligands	T (K)	n	K_b (x10^4) M^{-1}	K_{SV} (x10^3) M^{-1}
Quercetin (Q)	288	1.32 (± 0.27)	1.16 (± 0.40)	7.17 (± 0.36)
	298	0.98 (± 0.06)	1.03 (± 0.11)	8.25 (± 0.45)
	308	1.13 (± 0.04)	3.43 (± 0.22)	26.23 (± 0.56)
Peracetylated quercetin (Q1)	288	1.06 (± 0.10)	5.50 (± 0.80)	49.33 (± 1.54)
	298	1.22 (± 0.04)	8.50 (± 0.43)	72.75 (± 1.40)
	308	1.14 (± 0.01)	7.55 (± 0.19)	68.81 (± 2.46)
Tetraacetylated quercetin (Q2)	288	1.20 (± 0.03)	3.33 (± 0.15)	25.39 (± 0.36)
	298	0.93 (± 0.02)	2.74 (± 0.12)	23.97 (± 0.70)
	308	0.99 (± 0.03)	4.91 (± 0.26)	41.85 (± 0.88)

Analysis of the binding constants (Kb) showed that all compounds displayed values on the order of 10^4 M^{-1}. Such magnitudes are indicative of moderate binding affinity, which is nonetheless biologically relevant in the context of protein-ligand interactions [38,42]. Despite sharing the same order of magnitude, the constants exhibited discernible differences that allowed the establishment of a relative affinity hierarchy: Q1 > Q2 > Q [38,59]. Among the derivatives, peracetylated quercetin (Q1) consistently exhibited the highest binding constants across all tested temperatures, reaching 8.50 x 10^4 M^{-1} at 298 K [38]. Tetraacetylated quercetin (Q2) showed intermediate values (2.74 - 4.91 x 10^4 M^{-1}), whereas unmodified quercetin displayed comparatively lower binding, particularly at lower temperatures, although a marked increase was observed at 308 K (K_b = 3.43 x 10^4 M^{-1}) [38,42]. This behavior is consistent with the dynamic nature of the interaction suggested by Stern-Volmer analyses [57,60].

These differences directly reflect the impact of chemical modifications on binding affinity. In the case of Q1, the enhanced binding constant suggests that acetylation favors recognition promotes M protein, most likely through strengthening hydrophobic contacts and decreasing the overall polarity of the molecule [59,61]. Although Q2 did not reach the affinity levels observed for Q1, its values remained consistently higher than those of unmodified quercetin, implying that partial acetylation also enhances the interaction. This reinforces the notion that the degree of acetylation is a key determinant in modulating binding strength.

Another important aspect concerns the thermal behavior observed for quercetin, the sharp increase in both K_b and K_{SV} at 308 K indicates that binding is promoted by temperature-dependent mechanisms, compatible with dynamic quenching and transient contacts [57,62]. In contrast, Q1 and Q2 displayed relatively stable Kb values across the studied temperature range, which is more consistent with static quenching processes involving the formation of stable protein-ligand complexes [60,62].

c. COMPUTATIONAL EVALUATION OF INTERACTIONS

For the computational evaluation of ligand interactions, we selected the M protein protomer, which already provides the binding site to characterize the ligand interaction process.

In order to investigate the dynamic behavior and structural stability of the complexes formed between the M protein and the compounds Q, Q1 and Q2, molecular dynamics (MD) simulations were performed. These simulations were initiated from the lowest-energy conformations obtained through molecular docking analyses [63,64]. One of the key parameters used to monitor the stability of the systems over the course of the simulations was the root-mean-square deviation (RMSD), calculated based on the coordinates of the protein

backbone atoms [63,65,66]. For the ligands, RMSD values were determined through considering all heavy atoms [64,67]. The RMSD profiles of the unbound M protein (APO) and the protein in complex with the three ligands ($HOLO_Q$, $HOLO_{Q1}$ and $HOLO_{Q2}$) are presented in Figure 5A. The positional deviations of the ligands relative to their respective binding sites within the M protein are shown in Figure 5B. In general, the RMSD data indicates that the presence of the ligands does not compromise the conformational stability of the M protein throughout the simulation timescale (Figure 5A) [63]. Regarding the ligands themselves, all three compounds maintained stable interactions with the protein for the majority of the simulated trajectory (Figure 5B). However, the acetylated derivatives (Q1 and Q2) exhibited more consistent stability when compared to the unmodified quercetin. These findings agree with experimental data obtained via fluorescence spectroscopy (Figure 2), which also suggest a more favorable interaction between the M protein and the acetylated derivatives [38].

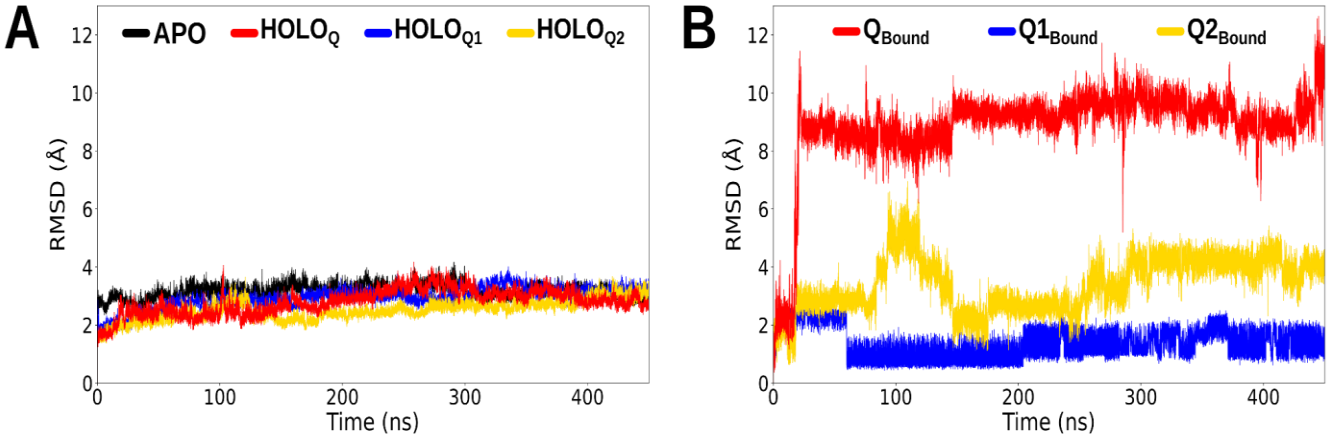

Figure 5: RMSD analysis of the hRSV M protein in different ligand-binding. **(A)** Temporal evolution of the RMSD for the APO system (ligand-free, black), HOLOQ (red), HOLOQ1 (blue), and HOLOQ2 (yellow). **(B)** RMSD of the ligands relative to their initial positions within the M protein binding site, used to assess the stability of the complexes.

As a complement to the structural stability analysis via RMSD, we performed root mean square fluctuation (RMSF) calculations to assess the local flexibility of the M protein residues throughout the simulations [64,66]. This approach enabled the identification of regions undergoing dynamic alterations in response to ligand binding. Mean RMSF values were obtained from three independent replicates for each system. Although Figure 6A presents the RMSF profiles directly, the comparative assessment between APO and HOLO states was still based on the residue-wise differences (APO - HOLO). In Figure 6A, these RMSF profiles are color-coded for clarity, red for $HOLO_Q$, blue for $HOLO_{Q1}$ and yellow for $HOLO_{Q2}$. Higher RMSF values indicate increased flexibility in a given state.

In summary, most residues exhibited reduced mobility in the presence of ligands, suggesting a stabilizing effect induced through complex formation [64,66]. A specific region spanning residues Leu133 to Thr137 displayed increased flexibility across all HOLO conditions, which may reflect local conformational adjustments driven via ligand interactions [10,68].

The highlighted residues (Figure 6B) show the most marked differences between the unbound and bound states. These residues were identified using the RMSF difference (APO - HOLO) and those showing consistent variations (RMSF differences > 0.5 Å) across all complexes are marked in green, while those exhibiting ligand-specific behaviors are shown in pink. Among these, Lys102, Leu133, Thr137, Thr177, Glu232 and Arg255 are notable for their differential responses to the ligands, potentially reflecting specific binding interactions or allosteric effects mediated by acetylation patterns in each derivative. All analyzed residues are comprehensively listed in Table S1. A complete list of residues categorized according to these criteria is available in the *Supporting Information* (Table S1).

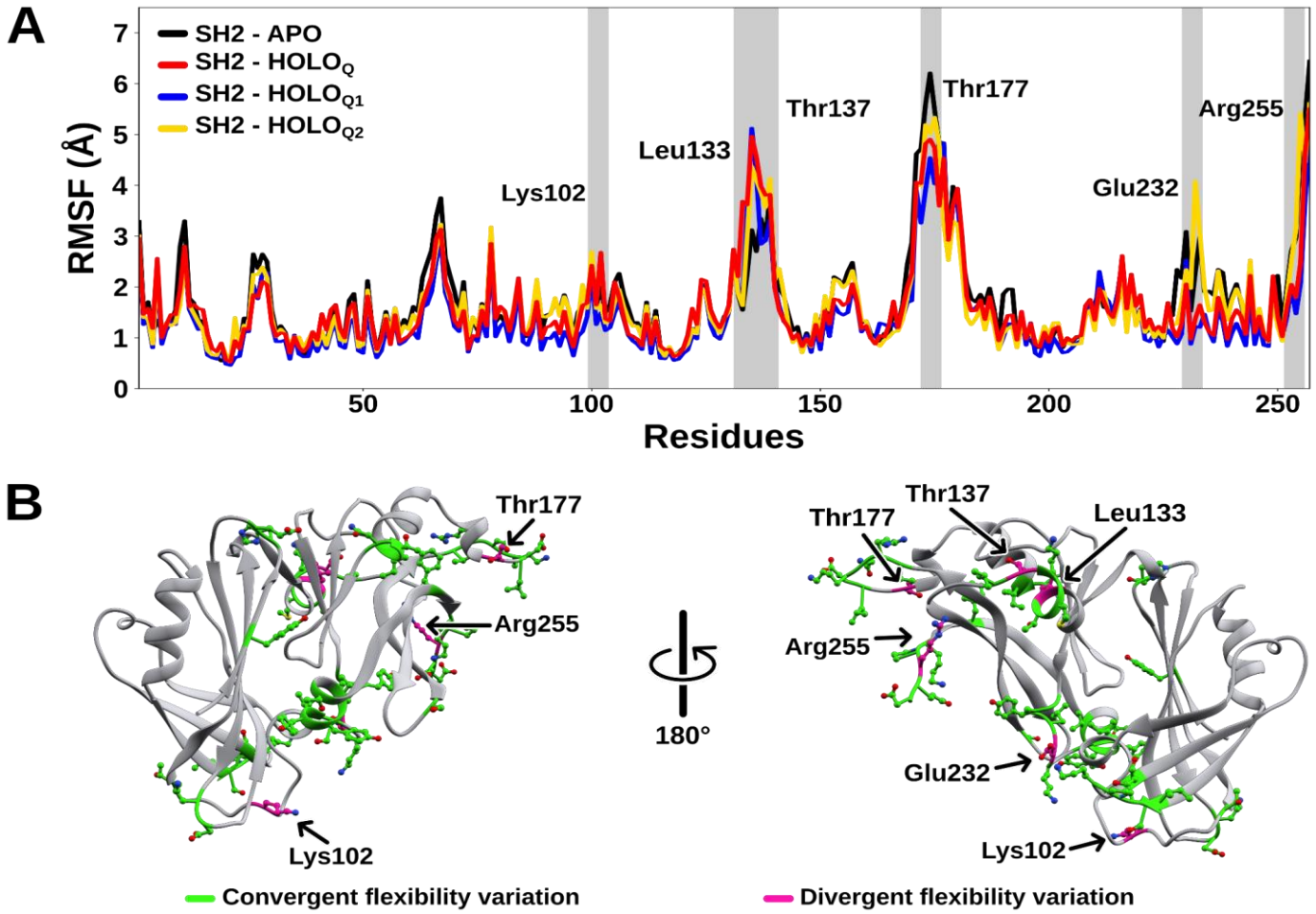

Figure 6: Flexibility of the M protein in complexes with quercetins. **(A)** RMSF profiles for APO state (black), complex with Q ($HOLO_Q$, red), Q1 ($HOLO_{Q1}$, blue) and Q2 ($HOLO_{Q2}$, yellow). **(B)** Changes mapped onto the M protein, green residues represent convergent responses to ligand binding, and magenta residues denote divergent flexibility patterns.

To better understand the potential functional consequences of the flexibility variations observed in the molecular dynamics simulations, we performed a comparative analysis between the protomer model of the M protein used in this computational part and its crystallographic dimeric structure (PDB ID: 4V23 [10]). The purpose of this comparison was to determine whether the residues showing significant fluctuations in the RMSF profiles (Table S1) correspond to regions previously reported as part of the dimerization interface. According to previous studies, the main residues forming this interface include Lys60, Thr63-Leu68, Ile71, Lys93, Leu96-Ile98, Ile104, Ala105, Gly129, Leu130, Leu133, Tyr142, Ser144, Ile159, Gly161, Val163, Gly228, Gly229, Ala231, Glu232 and Arg255. Notably, several of these residues also displayed pronounced differences in flexibility between the APO and HOLO forms, as indicated in Table S1 [10].

Structural inspection of the molecular dynamic complexes revealed, however, that the ligands do not bind directly to the dimerization interface. As illustrated in Figure 7, the binding pocket is located in a topologically distinct region that remains structurally connected to the interface through adjacent secondary structure elements. This spatial arrangement suggests that ligand binding may modulate the overall dynamics of the M protein through an allosteric mechanism, propagating conformational changes toward the dimerization interface [69,70].

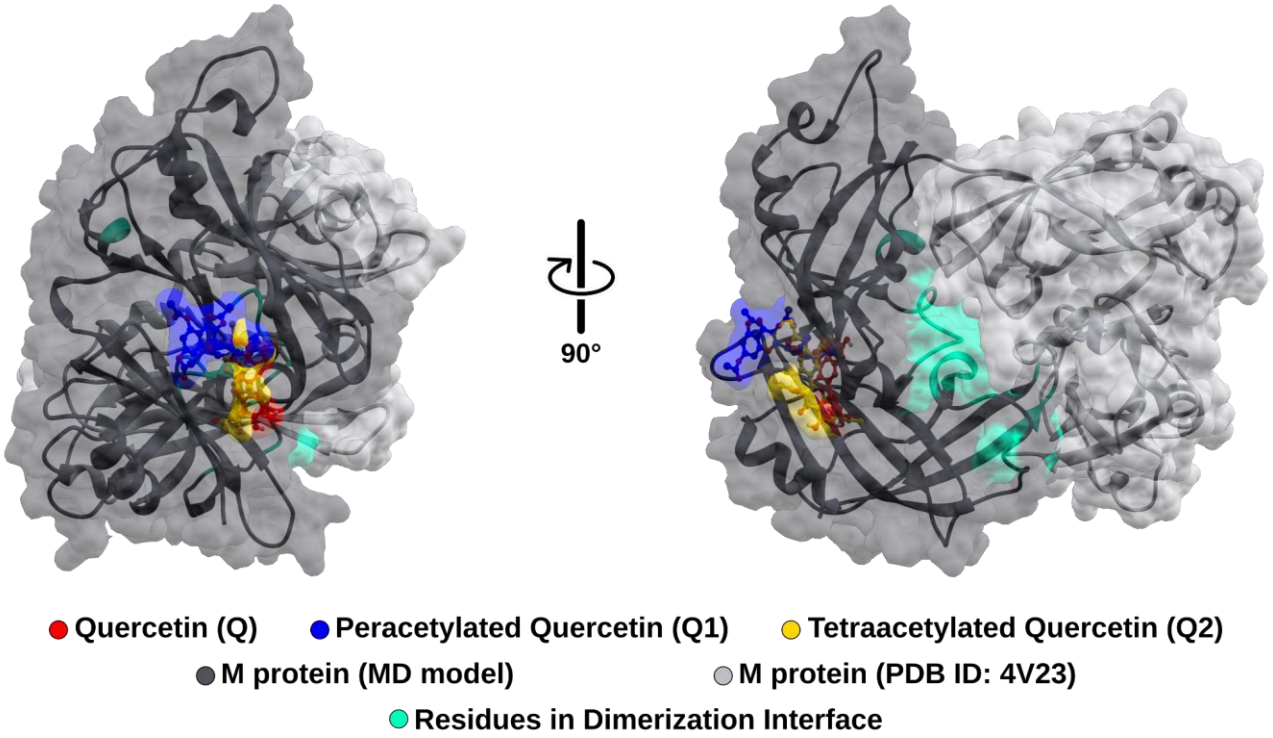

Figure 7: Structural comparison between the protomer model of the M protein (dark gray surface) and the crystallographic dimer (light gray surface). The binding sites of Q (red), Q1 (blue), and Q2 (yellow). Residues forming the dimerization interface are highlighted in aquamarine.

d. HYDROPHOBICITY AS A DETERMINING FACTOR IN MOLECULAR INTERACTION

Fluorescence experiments also enabled the characterization of the thermodynamic parameters governing the interaction between protein M and the different ligands. Based on the Van't Hoff equation (Eq. 4), the corresponding plots were constructed (Figure S2), from which the values of ΔH, ΔG and TΔS were derived at distinct experimental temperatures [71]. A summary of these results is presented in Table 2.

Table 2: Thermodynamic parameters (ΔH, ΔG and TΔS) associated with the interaction of protein M with Q, Q1, and Q2 at 288, 298, and 308 K.

Ligands	T (K)	ΔH kcal Mol^{-1}	ΔG kcal Mol^{-1}	TΔS kcal Mol^{-1}
Quercetin	288	9.40 (± 3.68)	-5.35 (± 1.84)	14.35 (± 10,72)
	298		-5.47 (± 0.58)	14.47 (± 7,31)
	308		-6.40 (± 0.40)	15.40 (± 7.12)
Peracetylated quercetin (Q1)	288	2.92 (± 0.48)	-6.25 (± 0.91)	9.16 (± 1.50)
	298		-6.72 (± 0.34)	9.64 (± 1.58)
	308		-6.87 (± 0.17)	9.80 (± 1.60)
Tetraacetylated quercetin (Q2)	288	3.57 (± 0.43)	-5.95 (± 0.27)	9.53 (± 1.60)
	298		-6.05 (± 0.26)	9.62 (± 1.60)
	308		-6.61 (± 0.35)	10.20 (± 1.78)

The negative ΔG values confirm the spontaneous nature of the association process under all experimental conditions [72]. However, the principal contribution to complex stabilization is entropic (TΔS), whose magnitude markedly outweighs the enthalpic term (ΔH). Such behavior is characteristic of processes predominantly driven by hydrophobic interactions, in which dehydration of the protein-ligand interface increases the overall entropy of the system [73,74].

When comparing the compounds, Q1 and Q2, display more consistent TΔS profiles across the temperatures investigated, whereas unmodified quercetin exhibits greater variation, consistent with the dynamic quenching mechanism proposed earlier. Graphical analysis (Figure 8) supports this distinction, indicating that acetylation strengthens protein-ligand association not only by enhancing hydrophobic contributions but also introducing novel, specific contact points [75,76].

In Figure 8, interaction diagrams generated with LigPlot, derived from the most representative conformations of the molecular dynamic trajectories, reveal that quercetin binds primarily through hydrophobic contacts, whereas the acetylated derivatives additionally establish hydrogen bonds, Q1 with Ile195 and Q2 with Ser117. These supplementary contacts account for the experimentally observed affinity hierarchy (Q1 > Q2 > quercetin) and are consistent with clustering analyses of the trajectories (Figure S1B), which revealed increased conformational stability for complexes containing the acetylated derivatives [36,59,75].

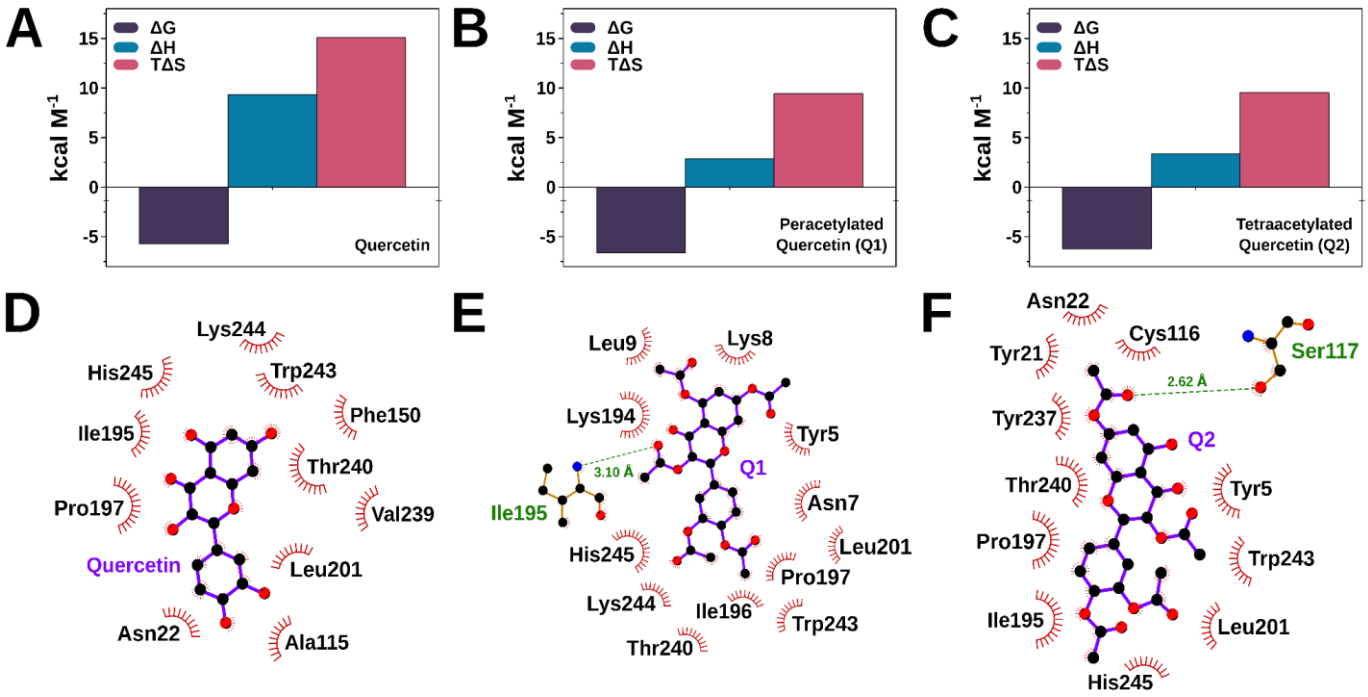

Figure 8: Bar plots of ΔH, ΔG and TΔS values for Q **(A)**, Q1 **(B)**, and Q2 **(C)** at 288, 298, and 308 K. Diagrams generated via LigPlot from the most representative conformations of the molecular dynamic simulations: Q1 **(D)**, Q1 **(E)**, and Q2 **(F)**. Hydrophobic interactions (green), with additional hydrogen bonds observed for Q1 (Ile195) and Q2 (Ser117).

4. Discussion

The comparative results showed that Q1 was the most effective quencher regardless of temperature, subsequent to Q2, whereas the quercetin scaffold had a significantly lower quenching efficacy. According to this hierarchy, acetylation probably increases hydrophobic surface area and permits more nonpolar interactions with the M protein, which increases ligand–protein contact [33,38]. In essence, the distinct quenching regimes observed dynamic quenching predominating for quercetin and a substantial static component for the acetylated derivatives [77] indicate that these molecules engage the M protein through divergent interaction modes.

These physicochemical distinctions are relevant when contextualized within the multifunctional role of the M protein in the RSV life cycle. As established in structural and cell-based studies, M functions as the central organizer of virion assembly, bridging the RNP complex to the viral membrane and coordinating interactions with the envelope glycoproteins F and G [68]. M also undergoes regulated nucleocytoplasmic trafficking, with nuclear accumulation suppressing host transcription early in infection and subsequent cytoplasmic export enabling virion morphogenesis [78,79]. Because both processes rely on precisely tuned conformational transitions, the formation of more stable ligand-bound complexes, as observed for Q1 and Q2, may influence the conformational dynamics required for M to execute these regulatory functions.

The enhanced quenching efficiency and reduced temperature dependence of Q1 and Q2 directly reflect stronger and more thermodynamically stable interactions, consistent with the predominance of hydrophobic forces that are also central to M oligomerization and membrane association [79,80]. Thus, acetylated derivatives may preferentially engage hydrophobic patches on M that participate in structural rearrangements essential for viral assembly, offering a mechanism rationale for the differential quenching behaviors detected [81].

Given that M orchestrates multiple macromolecular interactions, including contacts with the nucleocapsid, glycoproteins, lipid rafts, and cytoskeletal components [79,80] even subtle alterations in its conformational plasticity may disrupt the efficiency of virion assembly and budding [68]. The high stability of Q1 and Q2 bound complexes suggests that such interactions may persist under diverse intracellular conditions, with the potential to modulate M dimerization kinetics or the recruitment of assembly factors [62,68]. The binding parameter n remained close to 1 under all experimental conditions, indicating that each M protein chain preferentially accommodates a single ligand molecule [60,82]. This supports the existence of a specific and well-defined binding mechanism, rather than a diffuse interaction involving multiple low-affinity sites [60].

Our MD showing reduced flexibility in residues implicated in dimerization, despite the absence of direct ligand contact [69,83]. These findings are consistent with an allosteric restriction model, in which hydrophobic chemical modifications reinforce the transmission of dynamic constraints across the protein [38,61]. Because M dimerization is indispensable for filamentous virion formation [79,80], perturbing this conformational cycle could hinder productive budding.

Beyond structural roles, recent work demonstrates that M also acts as an antagonist of the type I interferon response through interacting with the host adaptor RACK1 (Receptor for activated C kinase 1), an adaptor protein recruited via specific signaling molecules to

regulate diverse cellular processes and viral infection [78]. This immunomodulatory activity requires discrete conformational states and stable protein–protein interfaces. Ligands that restrict M flexibility even when bound allosterically could impair ability of M protein to engage RACK1, thereby attenuating its ability to suppress antiviral signaling pathways.

All our findings suggest that hydrophobicity is an essential attribute in the binding of the hRSV M protein to ligands. However, acetylation does more than enhance binding strength it qualitatively reshapes the interaction landscape through introducing additional anchoring points that stabilize the ligand–protein complex [75,76]. These combined effects position acetylated quercetin derivatives as promising scaffolds for rational antiviral design, with the potential to simultaneously disrupt multiple structural and regulatory functions of M, including dimerization and membrane association.

5. Conclusion

Quercetin and its acetylated derivatives, Q1 and Q2, were found to interact with the M protein of the human respiratory syncytial virus with moderate yet biologically relevant affinities. These interactions are mainly driven by hydrophobic forces, and acetylation appears to play a critical role in enhancing conformational stability and strengthening intermolecular contacts. Among the analyzed compounds, Q1 exhibited the most stable complex formation and the highest number of molecular contacts, suggesting that the acetyl substitution pattern directly affects the molecular recognition of the M protein.

Molecular dynamics simulations showed that ligand binding stabilizes regions associated with the dimerization interface, suggesting a potential allosteric mechanism modulating M protein dimerization. This behavior aligns with previous experimental evidence demonstrating the virucidal activity of quercetin derivatives and their ability to downregulate F protein expression [33].

Our data indicates that quercetin and its acetylated derivatives may act at multiple stages of the hRSV replication cycle. Further antiviral studies focusing on the effects of these compounds on M protein-mediated viral assembly and particle release will be essential to validate the functional relevance of these interactions and to guide the rational design of optimized flavonoid-based therapeutics against hRSV.

Acknowledgement

We would like to express our sincere gratitude to the anonymous reviewers for their careful suggestions and constructive criticism, which undoubtedly contributed to the enhancement of this work. This study was supported by the National Council for Scientific and Technological Development (CNPq: 310898/2021-8, 317157/2023-0 and 305480/2024-3), the São Paulo Research Foundation (FAPESP: 2019/04646-9, 2022/01492-3 and 2022/13050-5) and the Research Pro-Rectory of São Paulo State University (PROPe/UNESP: 5545). This study made use of NMRbox: National Center for Biomolecular NMR Data Processing and Analysis, a Biomedical Technology Research Resource (BTRR), which is supported by NIH grant P41GM111135 (NIGMS).

Declaration of Competing Interest

The authors declare that they have no known competing financial interests or personal relationships that could have appeared to influence the work reported in this paper as potential competing interests.

Author Contributions

L.S., J.M.S., J.S.B. and M.S.S. performed experimental studies. R.P.P. and J.V.P. performed computer studies. L.O.R., M.A.F., Í.P.C. and F.P.S. designed the project and supervised the experimental and computer work. L.S., R.P.P., J.M.S., J.S.B., L.O.R., M.A.F., Í.P.C. and F.P.S. wrote the manuscript. L.S. and R.P.P. contributed equally as co-first authors. All authors contributed to the analysis and discussion and provided critical feedback.

References

1. Lucion MF, Del Valle Juárez M, Pejito MN, et al. Impact of COVID-19 on the circulation of respiratory viruses in a children's hospital: an expected absence. *Arch Argent Pediatr*. 2022;120(2):99-105. doi:10.5546/aap.2022.eng.99
2. Priante E, Cavicchiolo ME, Baraldi E. RSV infection and respiratory sequelae. *Minerva Pediatr*. 2018;70(6):623-633. doi:10.23736/s0026-4946.18.05327-6
3. Bénet T, Sánchez Picot V, Messaoudi M, et al. Microorganisms Associated With Pneumonia in Children <5 Years of Age in Developing and Emerging Countries: The GABRIEL Pneumonia Multicenter, Prospective, Case-Control Study. *Clin Infect Dis*. 2017;65(4):604-612. doi:10.1093/cid/cix378
4. Li Y, Wang X, Blau DM, et al. Global, regional, and national disease burden estimates of acute lower respiratory infections due to respiratory syncytial virus in children younger than 5 years in 2019: a systematic analysis. *The Lancet*. 2022;399(10340):2047-2064. doi:10.1016/S0140-6736(22)00478-0
5. Ramaekers K, Rector A, Cuypers L, Lemey P, Keyaerts E, Van Ranst M. Towards a unified classification for human respiratory syncytial virus genotypes. *Virus Evol*. 2020;6(2):veaa052. doi:10.1093/ve/veaa052
6. Kaler J, Hussain A, Patel K, Hernandez T, Ray S. Respiratory Syncytial Virus: A Comprehensive Review of Transmission, Pathophysiology, and Manifestation. *Cureus*. 2023;15(3):e36342. doi:10.7759/cureus.36342
7. Tawar RG, Duquerroy S, Vonrhein C, et al. Crystal Structure of a Nucleocapsid-Like Nucleoprotein-RNA Complex of Respiratory Syncytial Virus. *Science*. 2009;326(5957):1279-1283. doi:10.1126/science.1177634
8. Ke Z, Dillard RS, Chirkova T, et al. The Morphology and Assembly of Respiratory Syncytial Virus Revealed by Cryo-Electron Tomography. *Viruses*. 2018;10(8):446. doi:10.3390/v10080446
9. Rodrigues T, Busso J de S, Dias RVR, et al. Interaction of Human Respiratory Syncytial Virus (HRSV) Matrix Protein with Resveratrol Shows Antiviral Effect. *Int J Mol Sci*. 2024;25(23):12790. doi:10.3390/ijms252312790
10. Förster A, Maertens GN, Farrell PJ, Bajorek M. Dimerization of Matrix Protein Is Required for Budding of Respiratory Syncytial Virus. *J Virol*. 2015;89(8):4624-4635. doi:10.1128/jvi.03500-14
11. Bajorek M, Caly L, Tran KC, et al. The Thr205 Phosphorylation Site within Respiratory Syncytial Virus Matrix (M) Protein Modulates M Oligomerization and Virus Production. *J Virol*. 2014;88(11):6380-6393. doi:10.1128/jvi.03856-13
12. Hu M, Bogoyevitch MA, Jans DA. Impact of Respiratory Syncytial Virus Infection on Host Functions: Implications for Antiviral Strategies. *Physiol Rev*. 2020;100(4):1527-1594. doi:10.1152/physrev.00030.2019
13. Ghildyal R, Ho A, Wagstaff KM, et al. Nuclear Import of the Respiratory Syncytial Virus Matrix Protein Is Mediated By Importin β1 Independent of Importin α. *Biochemistry*. 2005;44(38):12887-12895. doi:10.1021/bi050701e
14. Ghildyal R, Baulch-Brown C, Mills J, Meanger J. The matrix protein of Human respiratory syncytial virus localises to the nucleus of infected cells and inhibits transcription. *Arch Virol*. 2003;148(7):1419-1429. doi:10.1007/s00705-003-0112-y
15. Ghildyal R, Mills J, Murray M, Vardaxis N, Meanger J. Respiratory syncytial virus matrix protein associates with nucleocapsids in infected cells. *J Gen Virol*. 2002;83(4):753-757. doi:10.1099/0022-1317-83-4-753
16. Li D, Jans DA, Bardin PG, Meanger J, Mills J, Ghildyal R. Association of Respiratory Syncytial Virus M Protein with Viral Nucleocapsids Is Mediated by the M2-1 Protein. *J Virol*. 2008;82(17):8863-8870. doi:10.1128/jvi.00343-08
17. Ghildyal R, Ho A, Dias M, et al. The Respiratory Syncytial Virus Matrix Protein Possesses a Crm1-Mediated Nuclear Export Mechanism. *J Virol*. 2009;83(11):5353-5362. doi:10.1128/jvi.02374-08
18. Mitra R, Baviskar P, Duncan-Decocq RR, Patel D, Oomens AGP. The Human Respiratory Syncytial Virus Matrix Protein Is Required for Maturation of Viral Filaments. *J Virol*. 2012;86(8):4432-4443. doi:10.1128/jvi.06744-11
19. Kipper S, Hamad S, Caly L, et al. New Host Factors Important for Respiratory Syncytial Virus (RSV) Replication Revealed by a Novel Microfluidics Screen for Interactors of Matrix (M) Protein *[S]. *Mol Cell Proteomics*. 2015;14(3):532-543. doi:10.1074/mcp.M114.044107
20. Ward C, Maselko M, Lupfer C, Prescott M, Pastey MK. Interaction of the Human Respiratory Syncytial Virus matrix protein with cellular adaptor protein complex 3 plays a critical role in trafficking. *PLOS ONE*. 2017;12(10):e0184629. doi:10.1371/journal.pone.0184629
21. Oliveira AP, Simabuco FM, Tamura RE, et al. Human respiratory syncytial virus N, P and M protein interactions in HEK-293T cells. *Virus Res*. 2013;177(1):108-112. doi:10.1016/j.virusres.2013.07.010
22. Domachowske JB, Anderson EJ, Goldstein M. The Future of Respiratory Syncytial Virus Disease Prevention and Treatment. *Infect Dis Ther*. 2021;10(1):47-60. doi:10.1007/s40121-020-00383-6
23. Anastassopoulou C, Medić S, Ferous S, Boufidou F, Tsakris A. Correction: Anastassopoulou et al. Development, Current Status, and Remaining Challenges for Respiratory Syncytial Virus Vaccines. Vaccines 2025, 13, 97. *Vaccines*. 2025;13(4):354. doi:10.3390/vaccines13040354
24. Research C for BE and. AREXVY. *FDA*. Published online August 8, 2025. Accessed September 1, 2025. https://www.fda.gov/vaccines-blood-biologics/arexvy
25. Bonneux B, Jacoby E, Ceconi M, Stobbelaar K, Delputte P, Herschke F. Direct-acting antivirals for RSV treatment, a review. *Antiviral Res*. 2024;229:105948. doi:10.1016/j.antiviral.2024.105948

26. Zakaryan H, Arabyan E, Oo A, Zandi K. Flavonoids: promising natural compounds against viral infections. *Arch Virol*. 2017;162(9):2539-2551. doi:10.1007/s00705-017-3417-y
27. Di Petrillo A, Orrù G, Fais A, Fantini MC. Quercetin and its derivates as antiviral potentials: A comprehensive review. *Phytother Res*. 2022;36(1): 266-278. doi:10.1002/ptr.7309
28. Yu YB, Miyashiro H, Nakamura N, Hattori M, Park JC. Effects of triterpenoids and flavonoids isolated from alnus firma on HIV-1 viral enzymes. *Arch Pharm Res*. 2007;30(7):820-826. doi:10.1007/BF02978831
29. Ganesan S, Faris AN, Comstock AT, et al. Quercetin inhibits rhinovirus replication *in vitro* and *in vivo*. *Antiviral Res*. 2012;94(3):258-271. doi:10.1016/j.antiviral.2012.03.005
30. Wu W, Li R, Li X, et al. Quercetin as an Antiviral Agent Inhibits Influenza A Virus (IAV) Entry. *Viruses*. 2016;8(1):6. doi:10.3390/v8010006
31. Kaul TN, Middleton Jr. E, Ogra PL. Antiviral effect of flavonoids on human viruses. *J Med Virol*. 1985;15(1):71-79. doi:10.1002/jmv.1890150110
32. Gomes DE, Caruso ÍP, Araujo GC de, et al. Experimental evidence and molecular modeling of the interaction between hRSV-NS1 and quercetin. *Int J Biol Macromol*. 2016;85:40-47. doi:10.1016/j.ijbiomac.2015.12.051
33. Lopes BRP, da Costa MF, Genova Ribeiro A, et al. Quercetin pentaacetate inhibits *in vitro* human respiratory syncytial virus adhesion. *Virus Res*. 2020;276:197805. doi:10.1016/j.virusres.2019.197805
34. Oteiza PI, Erlejman AG, Verstraeten SV, Keen CL, Fraga CG. Flavonoid-membrane Interactions: A Protective Role of Flavonoids at the Membrane Surface? *J Immunol Res*. 2005;12(1):592035. doi:10.1080/10446670410001722168
35. Wu T, He M, Zang X, et al. A structure–activity relationship study of flavonoids as inhibitors of *E. coli* by membrane interaction effect. *Biochim Biophys Acta BBA - Biomembr*. 2013;1828(11):2751-2756. doi:10.1016/j.bbamem.2013.07.029
36. Sakao K, Fujii M, Hou DX. Acetyl derivate of quercetin increases the sensitivity of human leukemia cells toward apoptosis. *BioFactors*. 2009;35(4):399-405. doi:10.1002/biof.53
37. Nettore IC, Rocca C, Mancino G, et al. Quercetin and its derivative Q2 modulate chromatin dynamics in adipogenesis and Q2 prevents obesity and metabolic disorders in rats. *J Nutr Biochem*. 2019;69:151-162. doi:10.1016/j.jnutbio.2019.03.019
38. Guimarães GC, Piva HRM, Araújo GC, et al. Binding investigation between M2-1protein from hRSV and acetylated quercetin derivatives: 1H NMR, fluorescence spectroscopy, and molecular docking. *Int J Biol Macromol*. 2018;111:33-38. doi:10.1016/j.ijbiomac.2017.12.141
39. Piva HMR, Sá JM, Miranda AS, et al. Insights into Interactions of Flavanones with Target Human Respiratory Syncytial Virus M2-1 Protein from STD-NMR, Fluorescence Spectroscopy, and Computational Simulations. *Int J Mol Sci*. 2020;21(6):2241. doi:10.3390/ijms21062241
40. Ottenio de Lourenço I, Toscano Pedroso Quintino E, Henrique Pereira M, et al. Biophysical studies of the interaction of hRSV Non-Structural 1 protein with natural flavonoids and their acetylated derivatives by spectroscopic techniques and computational simulations. *Spectrochim Acta A Mol Biomol Spectrosc*. 2022;283:121751. doi:10.1016/j.saa.2022.121751
41. Gold V, McNaught A, The International Union of Pure and Applied Chemistry (IUPAC), eds. *The IUPAC Compendium of Chemical Terminology: The Gold Book*. 5th ed. International Union of Pure and Applied Chemistry (IUPAC); 2025. doi:10.1351/goldbook
42. Machado VB, Sá JM de, Prado AKM, et al. Biophysical and flavonoid-binding studies of the G protein ectodomain of group A human respiratory syncytial virus. *Heliyon*. 2019;5(3). doi:10.1016/j.heliyon.2019.e01394
43. Guimarães GC, Machado VB, Sá JM de, Fossey MA, Caruso ÍP, Souza FP de. Characterization of the Thermal and Chemical Denaturation of the Matrix Protein from hRSV. *Biophys J*. 2020;118(3):358a-359a. doi:10.1016/j.bpj.2019.11.2065
44. Kumar Panigrahi S, Kumar Mishra A. Inner filter effect in fluorescence spectroscopy: As a problem and as a solution. *J Photochem Photobiol C Photochem Rev*. 2019;41:100318. doi:10.1016/j.jphotochemrev.2019.100318
45. Liu Y, Yang X, Gan J, Chen S, Xiao ZX, Cao Y. CB-Dock2: improved protein–ligand blind docking by integrating cavity detection, docking and homologous template fitting. *Nucleic Acids Res*. 2022;50(W1):W159-W164. doi:10.1093/nar/gkac394
46. Yang X, Liu Y, Gan J, Xiao ZX, Cao Y. FitDock: protein–ligand docking by template fitting. *Brief Bioinform*. 2022;23(3):bbac087. doi:10.1093/bib/bbac087
47. Money VA, McPhee HK, Mosely JA, Sanderson JM, Yeo RP. Surface features of a Mononegavirales matrix protein indicate sites of membrane interaction. *Proc Natl Acad Sci*. 2009;106(11):4441-4446. doi:10.1073/pnas.0805740106
48. Jo S, Kim T, Iyer VG, Im W. CHARMM-GUI: A web-based graphical user interface for CHARMM. *J Comput Chem*. 2008;29(11):1859-1865. doi:10.1002/jcc.20945
49. Kim S, Lee J, Jo S, Brooks III CL, Lee HS, Im W. CHARMM-GUI ligand reader and modeler for CHARMM force field generation of small molecules. *J Comput Chem*. 2017;38(21):1879-1886. doi:10.1002/jcc.24829
50. Lindahl, Abraham, Hess, Spoel van der. GROMACS 2020.3 Manual. Published online July 9, 2020. doi:10.5281/zenodo.3923644
51. Huang J, MacKerell AD. CHARMM36 all-atom additive protein force field: validation based on comparison to NMR data. *J Comput Chem*. 2013;34(25):2135-2145. doi:10.1002/jcc.23354
52. Vanommeslaeghe K, MacKerell AD. CHARMM additive and polarizable force fields for biophysics and computer-aided drug design. *Biochim Biophys Acta BBA - Gen Subj*. 2015;1850(5):861-871. doi:10.1016/j.bbagen.2014.08.004
53. Jorgensen WL, Chandrasekhar J, Madura JD, Impey RW, Klein ML. Comparison of simple potential

functions for simulating liquid water. *J Chem Phys*. 1983;79(2):926-935. doi:10.1063/1.445869
54. Berendsen HJC. Transport Properties Computed by Linear Response through Weak Coupling to a Bath. In: Meyer M, Pontikis V, eds. *Computer Simulation in Materials Science: Interatomic Potentials, Simulation Techniques and Applications*. NATO ASI Series. Springer Netherlands; 1991:139-155. doi:10.1007/978-94-011-3546-7_7
55. Parrinello M, Rahman A. Polymorphic transitions in single crystals: A new molecular dynamics method. *J Appl Phys*. 1981;52(12):7182-7190. doi:10.1063/1.328693
56. Tayeh N, Rungassamy T, Albani JR. Fluorescence spectral resolution of tryptophan residues in bovine and human serum albumins. *J Pharm Biomed Anal*. 2009;50(2):107-116. doi:10.1016/j.jpba.2009.03.015
57. Lakowicz JR, ed. Instrumentation for Fluorescence Spectroscopy. In: *Principles of Fluorescence Spectroscopy*. Springer US; 2006:27-61. doi:10.1007/978-0-387-46312-4_2
58. Bi S, Ding L, Tian Y, et al. Investigation of the interaction between flavonoids and human serum albumin. *J Mol Struct*. 2004;703(1):37-45. doi:10.1016/j.molstruc.2004.05.026
59. Sakao K, Saruwatari H, Minami S, Hou DX. Hydroxyl Group Acetylation of Quercetin Enhances Intracellular Absorption and Persistence to Upregulate Anticancer Activity in HepG2 Cells. *Int J Mol Sci*. 2023;24(23):16652. doi:10.3390/ijms242316652
60. dos Santos Rodrigues FH, Delgado GG, Santana da Costa T, Tasic L. Applications of fluorescence spectroscopy in protein conformational changes and intermolecular contacts. *BBA Adv*. 2023;3:100091. doi:10.1016/j.bbadva.2023.100091
61. Essa AF, Teleb M, El-Kersh DM, El Gendy AENG, Elshamy AI, Farag MA. Natural acylated flavonoids: their chemistry and biological merits in context to molecular docking studies. *Phytochem Rev*. 2023;22(6):1469-1508. doi:10.1007/s11101-022-09840-1
62. Fossum CJ, Johnson BOV, Golde ST, et al. Insights into the Mechanism of Tryptophan Fluorescence Quenching due to Synthetic Crowding Agents: A Combined Experimental and Computational Study. *ACS Omega*. 2023;8(47):44820-44830. doi:10.1021/acsomega.3c06006
63. Salo-Ahen OMH, Alanko I, Bhadane R, et al. Molecular Dynamics Simulations in Drug Discovery and Pharmaceutical Development. *Processes*. 2021; 9(1):71. doi:10.3390/pr9010071
64. Chao P, Zhang X, Zhang L, Yang A, Wang Y, Chen X. Integration of molecular docking and molecular dynamics simulations with subtractive proteomics approach to identify the novel drug targets and their inhibitors in Streptococcus gallolyticus. *Sci Rep*. 2024;14(1):14755. doi:10.1038/s41598-024-64769-z
65. Fani N, Bordbar AK, Ghayeb Y. Spectroscopic, docking and molecular dynamics simulation studies on the interaction of two Schiff base complexes with human serum albumin. *J Lumin*. 2013;141:166-172. doi:10.1016/j.jlumin.2013.03.001
66. Lemkul JA. Introductory Tutorials for Simulating Protein Dynamics with GROMACS. *J Phys Chem B*. 2024;128(39):9418-9435. doi:10.1021/acs.jpcb.4c04901
67. Fusani L, Palmer DS, Somers DO, Wall ID. Exploring Ligand Stability in Protein Crystal Structures Using Binding Pose Metadynamics. *J Chem Inf Model*. 2020;60(3):1528-1539. doi:10.1021/acs.jcim.9b00843
68. Sibert BS, Kim JY, Yang JE, et al. Assembly of respiratory syncytial virus matrix protein lattice and its coordination with fusion glycoprotein trimers. *Nat Commun*. 2024;15(1):5923. doi:10.1038/s41467-024-50162-x
69. Thayer KM, Lakhani B, Beveridge DL. Molecular Dynamics–Markov State Model of Protein Ligand Binding and Allostery in CRIB-PDZ: Conformational Selection and Induced Fit. *J Phys Chem B*. 2017;121(22):5509-5514. doi:10.1021/acs.jpcb.7b02083
70. Abrusán G, Marsh JA. Ligand-Binding-Site Structure Shapes Allosteric Signal Transduction and the Evolution of Allostery in Protein Complexes. *Mol Biol Evol*. 2019;36(8):1711-1727. doi:10.1093/molbev/msz093
71. Du X, Li Y, Xia YL, et al. Insights into Protein–Ligand Interactions: Mechanisms, Models, and Methods. *Int J Mol Sci*. 2016;17(2):144. doi:10.3390/ijms17020144
72. Olsson TSG, Ladbury JE, Pitt WR, Williams MA. Extent of enthalpy–entropy compensation in protein–ligand interactions. *Protein Sci*. 2011;20(9):1607-1618. doi:10.1002/pro.692
73. Olsson TSG, Williams MA, Pitt WR, Ladbury JE. The Thermodynamics of Protein–Ligand Interaction and Solvation: Insights for Ligand Design. *J Mol Biol*. 2008;384(4):1002-1017. doi:10.1016/j.jmb.2008.09.073
74. Syme NR, Dennis C, Bronowska A, Paesen GC, Homans SW. Comparison of Entropic Contributions to Binding in a "Hydrophilic" versus "Hydrophobic" Ligand−Protein Interaction. *J Am Chem Soc*. 2010;132(25):8682-8689. doi:10.1021/ja101362u
75. Das S, Bora N, Ataur Rohman M, Sharma R, Nath Jha A, Roy AS. Molecular recognition of bio-active flavonoids quercetin and rutin by bovine hemoglobin: an overview of the binding mechanism, thermodynamics and structural aspects through multi-spectroscopic and molecular dynamics simulation studies. *Phys Chem Chem Phys*. 2018;20(33):21668-21684. doi:10.1039/C8CP02760A
76. Martin SF, Clements JH. Correlating Structure and Energetics in Protein-Ligand Interactions: Paradigms and Paradoxes. *Annu Rev Biochem*. 2013;82(Volume 82, 2013):267-293. doi:10.1146/annurev-biochem-060410-105819
77. Pandey V, Pandey T. Spectroscopic Visualization of Drug–Biomolecules Interactions: An Insight to Fluorescence Quenching as Tool in Drug Discovery. *Luminescence*. 2025;40(4):e70168. doi:10.1002/bio.70168
78. Cao J, Shi M, Zhu L, et al. The matrix protein of respiratory syncytial virus suppresses interferon signaling via RACK1 association. *J Virol*.

2023;97(10):e00747-23. doi:10.1128/jvi.00747-23
79. Hu M, Bogoyevitch MA, Jans DA. Respiratory Syncytial Virus Matrix Protein Is Sufficient and Necessary to Remodel Host Mitochondria in Infection. *Cells*. 2023;12(9):1311. doi:10.3390/cells12091311
80. Li HM, Ghildyal R, Hu M, et al. Respiratory Syncytial Virus Matrix Protein-Chromatin Association Is Key to Transcriptional Inhibition in Infected Cells. *Cells*. 2021;10(10):2786. doi:10.3390/cells10102786
81. Roy AV, Chan M, Banadyga L, et al. Quercetin inhibits SARS-CoV-2 infection and prevents syncytium formation by cells co-expressing the viral spike protein and human ACE2. *Virol J*. 2024;21(1):29. doi:10.1186/s12985-024-02299-w
82. Jalali E, Sargolzaei J. Protocol for evaluating drug-protein interactions based on fluorescence spectroscopy. *STAR Protoc*. 2024;5(4):103429. doi:10.1016/j.xpro.2024.103429
83. Lamim Ribeiro JM, Filizola M. Allostery in G protein-coupled receptors investigated by molecular dynamics simulations. *Curr Opin Struct Biol*. 2019;55:121-128. doi:10.1016/j.sbi.2019.03.016

Supporting Information

Table S1: RMSF differences when comparing protein M (APO) with complexes (HOLO) Q, Q1, and Q2. Positive ΔRMSF (> 0.5 Å) indicate increased rigidity in the interaction, and negative (< -0.5 Å) suggest flexible region. Green residues denote structurally sensitive regions potentially critical for the stability of protein. Not highlighted residues reflect ligand-specific interactions

	$HOLO_{Quercetin}$			$HOLO_{Q1}$			$HOLO_{Q2}$		
ΔRMSF < -0.5 Å	Tyr5	Lys102	Leu133	Tyr5	Thr134	Met135	Tyr5	Asn22	Thr134
	Thr134	Met135	Lys136	Lys136	Thr177		Met135	Lys136	Thr137
	Thr137	Leu138	Thr177				Leu138	Glu232	Arg255
ΔRMSF > 0.5 Å	His10	Lys26	Asp27	His10	Glu11	Lys26	His10	Glu11	Ser64
	Asp28	Ile63	Ser64	Asp27	Lys51	Lys61	Thr65	Pro66	Lys67
	Thr65	Lys67	Ser70	Gln62	Ile63	Ser64	Ser169	Val170	Arg171
	Arg72	Thr108	Ser156	Thr65	Pro66	Lys67	Asn172	Asp174	Thr177
	Val170	Arg171	Asn172	Gly68	Pro69	Ser70	Glu179	Asn180	Thr182
	Lys173	Asp174	Leu175	Cys92	Ala93	Asn94	Thr183	Phe186	Ile190
	Asn176	Ile190	Thr191	Val95	Asp98	Lys102	Thr191	Asn192	Asn210
	Asn192	Gly228	Ala229	Tyr105	Asp106	Thr108	Gly228	Tyr230	Phe250
	Tyr230	Leu231	Glu232	Thr137	Ile153	Val154	Glu256	Asp257	
	Lys233	Glu234	Ser235	Thr155	Ser156	Ser169			
	Ile236	Tyr237	Tyr238	Val170	Arg171	Asn172			
	Val239	Thr241	Phe250	Lys173	Asp174	Leu175			
	Lys253	Pro254	Arg255	Ile190	Thr191	Asn192			
	Glu256	Asp257		Gly228	Ala229	Tyr230			
				Leu231	Glu232	Lys233			
				Ser235	Ile236	Tyr237			
				Tyr238	Val239	Thr240			
				Thr241	Asn242	Lys244			
				Phe250	Ile252	Lys253			
				Pro254	Arg255	Glu256			
				Asp257					

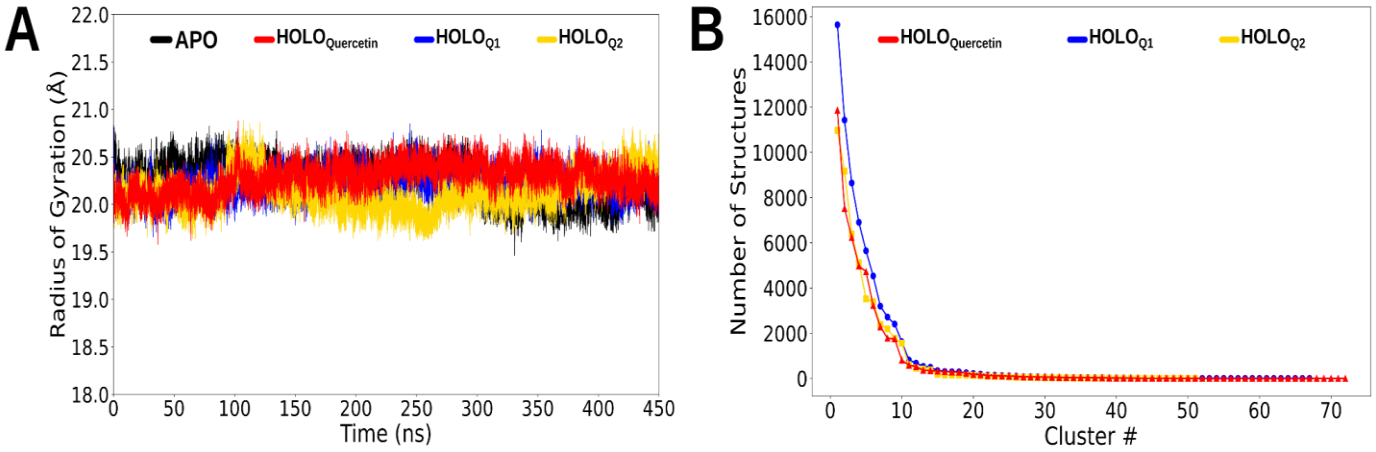

Figure S1: Structural comparison of the M protein in its unbound and ligand-bound forms. **(A)** Radius of Gyration of the M protein in its APO (black) form and in HOLO states Q (red), Q1 (blue), and Q2 (yellow). **(B)** Distribution of the predominant conformational states of the M protein/ligand complexes, obtained via clustering analysis of the simulation trajectories.

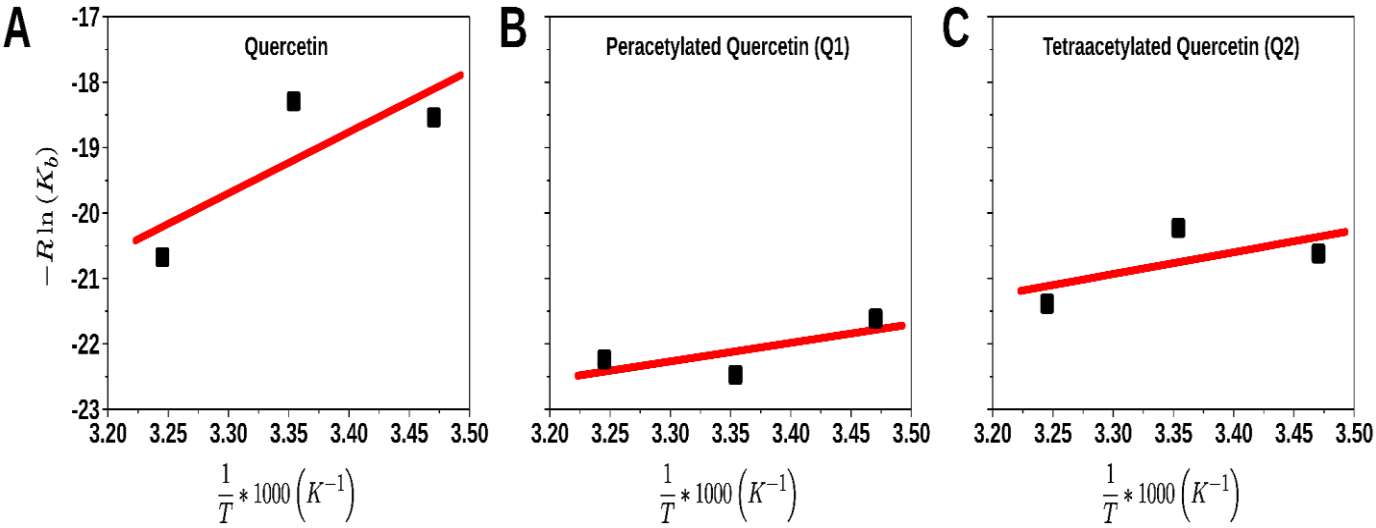

Figure S2: Van't Hoff plots derived from fluorescence measurements of the hRSV M protein in the presence of three ligands: Q **(A)**, Q1 **(B)**, and Q2 **(C)**. Red lines represent the linear fitting of the experimental data, shown as black dots.